NANOSYSTEMS:
PHYSICS, CHEMISTRY, MATHEMATICS

Zaitseva O.V., Trofimov E.A., et al. *Nanosystems: Phys. Chem. Math.*, 2023, **14** (3), 354–362.
http://nanojournal.ifmo.ru
DOI 10.17586/2220-8054-2023-14-3-354-362

Original article

Synthesis of $PbFe_{2.4}X_{2.4}Y_{2.4}Ga_{2.4}In_{2.4}O_{19}$ high-entropy oxides with the magnetoplumbite structure

Olga V. Zaitseva, Evgeny A. Trofimov, Vladimir E. Zhivulin, Ahmad Ostovari Mogaddam, Olga V. Samoilova, Ksenia S. Litvinyuk, Alena R. Zykova, Dmitry V. Mikhailov, Svetlana A. Gudkova, Denis A. Vinnik

South Ural State University, Chelyabinsk, Russia

Corresponding author: Denis A. Vinnik, vinnikda@susu.ru

ABSTRACT The purpose of this study is to obtain high-entropy oxides with the magnetoplumbite structure, in which the Pb cation is used as a divalent metal cation. The synthesis conditions were optimized, and a technique was developed to avoid the evaporation of lead oxide. For the first time, single-phase samples of high-entropy oxides with the magnetoplumbite structure were obtained, its chemical composition is reflected by the formula $PbFe_{2.4}X_{2.4}Y_{2.4}Ga_{2.4}In_{2.4}O_{19}$. The particle size of the high-entropy phase is about 100 nm, which makes it promising for a number of applications. The effect of preliminary grinding of the initial components on the results of synthesis was studied. A synthesis mechanism is proposed. The results pave the way to synthesis and study of the properties of a new large subgroup of high-entropy oxides with the magnetoplumbite structure, which expands the possibilities of controlling the properties of ceramic magnetic materials.

KEYWORDS high-entropy oxides, magnetoplumbite, lead, nanocrystals, structure, synthesis, magnetic materials

ACKNOWLEDGEMENTS This work was supported by the Russian Science Foundation (project No. 18-73-10049).

FOR CITATION Zaitseva O.V., Trofimov E.A., Zhivulin V.E., Ostovari Mogaddam A., Samoilova O.V., Litvinyuk K.S., Zykova A.R., Mikhailov D.V., Gudkova S.A., Vinnik D.A. Synthesis of $PbFe_{2.4}X_{2.4}Y_{2.4}Ga_{2.4}In_{2.4}O_{19}$ high-entropy oxides with the magnetoplumbite structure. *Nanosystems: Phys. Chem. Math.*, 2023, **14** (3), 354–362.

1. Introduction

Ferrites with the magnetoplumbite structure (with the space group $P6_3/mmc$) have been successfully used for a long time in the manufacturing of high-frequency transformers, fabricating of microwave electronic devices, and manufacturing of magnetic memory devices. They are also used in the manufacturing of functional sensors, as well as for the production of plastoferrites, magnetic fluids, permanent magnets, and multiferroics [1–14]. All these are possible due to the unique structural and magnetic properties of ferrites with the magnetoplumbite structure, as well as their mechanical, chemical and thermal resistance.

The level of development of modern technology imposes ever more stringent requirements on the materials used for manufacturing of devices. Such requirements for the performance of materials with the magnetoplumbite structure led to the idea of replacing some of the iron atoms in their structure with atoms of other elements. It was found that such a substitution leads to a change not only in the characteristics of the crystal lattice, but also in the properties of the resulting material, including changes in the magnitude of the coercive force, the Curie temperature, and the degree of uniaxial magnetic anisotropy. Thus, atomic substitution allows one to regulate the properties of materials in the required directions owing to the controlled changes in the qualitative and quantitative composition of dopants.

To date, a large number of works have been devoted to the study of the effect of Fe^{3+} ions substitution in the parent ferrites having a magnetoplumbite structure with the cations of other (most often, trivalent) metals. The elements acting as dopants include gallium [15], aluminum [16, 17], chromium [18], tin [4], indium [19], titanium [20], etc. Quite often, cobalt acts as a doping element [21].

However, the solubility of individual dopant elements in the ferrite structure and the ability of their atoms to occupy iron positions is, as a rule, limited. There are applications that require ceramics with a magnetoplumbite structure and a high (more than 50 at.%) degree of replacement of iron atoms by atoms of other elements. Obtaining such structures with one iron-replacing element is not feasible for all possible dopants. However, the formation of stable crystal structures with a high level of dopants can be facilitated by the high configurational entropy of mixing of the sublattice components, which is formed by iron atoms in magnetoplumbite and similar substances. High values of this quantity increase the entropy of the oxide phase as a whole, resulting in a decrease in its Gibbs free energy, and consequently, make the formation and existence of such a single-phase oxide more thermodynamically probable than the emergence of other substances from the same elements.

The concept of high-entropy phases arose in early 21st century, primarily in relation to metallic materials (such work is still relevant today, for example [22]), but since 2015 this concept has been actively and effectively developed for obtaining new nonmetallic phases (for example [23]) including ceramic phases. To date, high-entropy oxides (HEO) with various structures (such as spinel structure [24], perovskite structure [25], garnet structure [26], etc.) have been obtained. In our work, for the first time, stable high-entropy oxides with the magnetoplumbite structure were obtained [27–31], in which the iron ions were replaced mainly by ions of trivalent elements or pairs of bi- and tetravalent elements (to maintain electronic balance). An assessment is made of how the change in the entropy of mixing correlates with the changes in electrical and magnetic properties of a number of representatives of this new group of materials.

Previous studies [14] indicated that properties of oxide materials with the magnetoplumbite structure are determined not only by the qualitative and quantitative composition of the sublattice occupied by iron atoms and dopants, but also by the atom constituting a doubly charged cation outside this sublattice [14, 32]. To date, structures with Ba or Sr as such adoubly charged cation have been studied. Expanding the range of possible structures by increasing the number of such elements will increase the possibilities for expanding the range of variation in the magnetic and microwave properties of materials with the magnetoplumbite structure. An obvious candidate for such an element is Pb.

However, attempts to obtain and study high-entropy oxides with the magnetoplumbite structure, in which only lead would act as a divalent element, have so far been unsuccessful. Our attempts to obtain (Ba,Sr,Pb)$M_{12}O_{19}$ structures by solid-phase synthesis route at 1300 – 1400 °C ran into the fact that after calcination at these temperatures for 5 hours (the usual method for obtaining HEO with the magnetoplumbite structure with the participation of divalent metal Ba and Sr) magnetoplumbite structure was absent in the obtained Pb samples. At the same time, our results demonstrate that it is impossible to obtain single-phase HEOs with the magnetoplumbite structure with the participation of Ba or Sr during 5 hours at lower temperatures.

Therefore, the purpose of this study is to obtain HEO with the magnetoplumbite structure, in which Pb is used as a divalent metal cation. Considering the unsuccessful attempts to obtain magnetoplumbite phases at temperatures of 1300 – 1400 °C, it can be assumed that successful synthesis can be carried out at significantly lower temperatures and in a shorter time (to avoid evaporation of lead oxide). In this case, the success of the synthesis can be facilitated by more thorough grinding of the starting components.

A decrease in the synthesis temperature of HEO with the magnetoplumbite structure can facilitate the formation of the target phase in the form of smaller particles than that obtaining in the conventional process. Reducing the particle size down to nanosize, in turn, opens up the possibility of expanding the scope of possible applications of these substances not only as magnetic materials, but also as catalysts for oxidation/reduction processes.

Considering the phase diagram of PbO–Fe_2O_3 system [33] (Fig. 1), it can be assumed that during the synthesis, one should focus on the temperatures ranging from 886 – 1315 °C. The first temperature is the melting point of PbO and, at the same time, the minimum temperature at which the melt is in equilibrium with $PbFe_{12}O_{19}$. The second temperature is the temperature of the incongruent decomposition of $PbFe_{12}O_{19}$. Of course, it should be considered that, for high-entropy oxides, the temperatures of the last two processes can differ significantly from the temperatures in the PbO–Fe_2O_3 binary system, and that, in order to avoid losses of PbO, one should not increase the temperature above the minimum required for synthesis. Based on these considerations, the temperature regime used in the course of the experimental study was selected.

2. Methodology of experimental research

Oxides of iron Fe_2O_3, aluminum Al_2O_3, chromium Cr_2O_3, cobalt CoO, copper CuO, titanium TiO_2, tin SnO_2, gallium Ga_2O_3, indium In_2O_3, and lead PbO were used as starting components. All components were chemically pure. Table1 shows the chemical formulas of the target compounds and the mass content of the starting components. The compositions are chosen in such a way to ensure the maximum configurational entropy of mixing at the magnetoplumbite sublattice occupied by iron atoms ($\Delta S_{\mathrm{mix(B)}}$). According to the formula:

$$\Delta S_{\mathrm{mix(B)}} = -R\Sigma(x_{(\mathrm{B})} \ln x_{(\mathrm{B})}), \tag{1}$$

where $x_{(\mathrm{B})}$ is the atomic ratio of various cations filling sublattice B in $AB_{12}O_{19}$ unit cell, for a sublattice with five components presented in equimolar concentrations, this value is $1.6094R$ J/(mol·K).

The expected chemical reactions can be represented as the following equations:

$$\mathrm{PbO} + 6\mathrm{Fe_2O_3} \longrightarrow \mathrm{PbFe_{12}O_{19}}, \tag{2}$$

$$\mathrm{PbO} + \frac{6}{5}\mathrm{Cr_2O_3} + \frac{6}{5}\mathrm{Al_2O_3} + \frac{6}{5}\mathrm{In_2O_3} + \frac{6}{5}\mathrm{Ga_2O_3} + \frac{6}{5}\mathrm{Fe_2O_3} \longrightarrow \mathrm{PbFe_{2.4}Al_{2.4}Cr_{2.4}Ga_{2.4}In_{2.4}O_{10}}, \tag{3}$$

$$\mathrm{PbO} + \frac{12}{5}\mathrm{CoO} + \frac{12}{5}\mathrm{TiO_2} + \frac{6}{5}\mathrm{In_2O_3} + \frac{6}{5}\mathrm{Ga_2O_3} + \frac{6}{5}\mathrm{Fe_2O_3} \longrightarrow \mathrm{PbFe_{2.4}Co_{2.4}Ti_{2.4}Ga_{2.4}In_{2.4}O_{19}}, \tag{4}$$

$$\mathrm{PbO} + \frac{12}{5}\mathrm{CuO} + \frac{12}{5}\mathrm{SnO_2} + \frac{6}{5}\mathrm{In_2O_3} + \frac{6}{5}\mathrm{Ga_2O_3} + \frac{6}{5}\mathrm{Fe_2O_3} \longrightarrow \mathrm{PbFe_{2.4}Cu_{2.4}Sn_{2.4}Ga_{2.4}In_{2.4}O_{19}}. \tag{5}$$

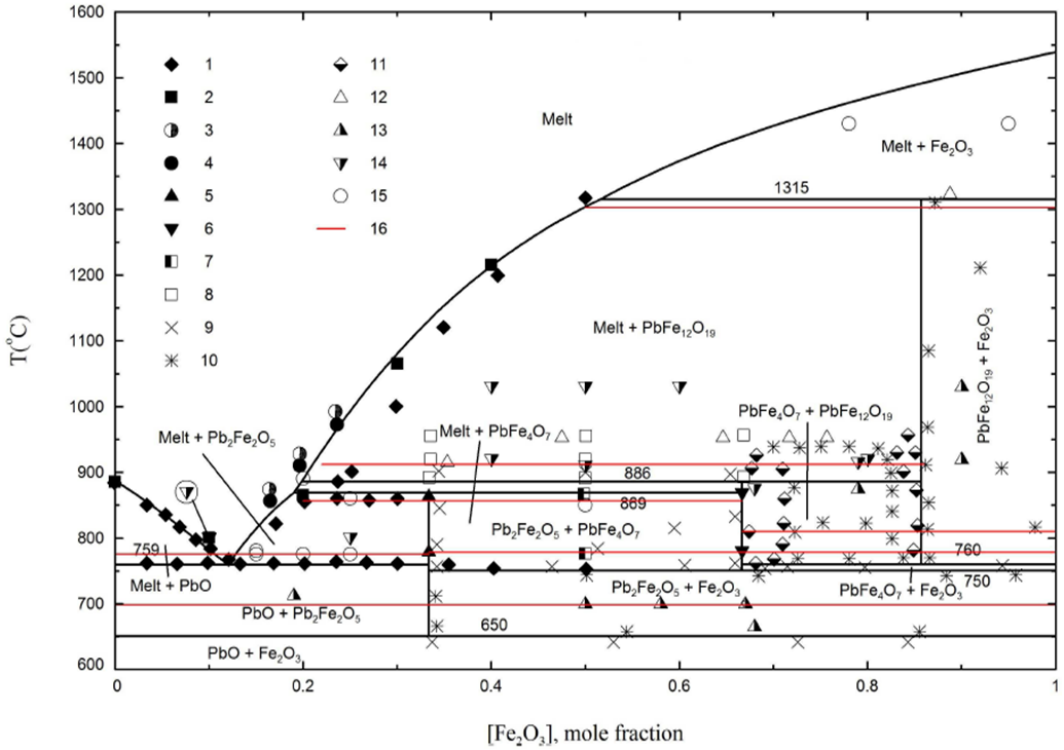

FIG. 1. Phase diagram of the PbO–Fe_2O_3 system [33]. 1 – DTA [34], 2 – DTA [35], 3 and 4 – liquidus temperature data [34], 5 – XRD ($Pb_2Fe_2O_5$) [34], 6 – XRD ($PbFe_4O_7$) [34], 7 – XRD ($Pb_2Fe_2O_5$+$PbFe_4O_7$) [34], 8 – XRD (PbO+$PbFe_{12}O_{19}$) [34], 9 and 10 – two solid phases [36], 11 – one solid phase [36], 12 – melt and solid phase [36], 13 – SEM, two solid phases [37], 14 – SEM, melt and solid phase [37], 15 – DTA, [33], 16 – average results DTA, obtained in the work [37]

TABLE 1. Compositions of initial mixtures

#	Chemical formula	Composition, wt. %					
		PbO	Al_2O_3/CoO/CuO	Cr_2O_3/TiO_2/SnO_2	Ga_2O_3	In_2O_3	Fe_2O_3
1	$PbFe_{12}O_{19}$	18.894	—	—	—	—	81.106
2	$PbFe_{2.4}Al_{2.4}Cr_{2.4}Ga_{2.4}In_{2.4}O_{19}$	17.736	9.722	14.493	17.874	24.948	15.227
3	$PbFe_{2.4}Co_{2.4}Ti_{2.4}Ga_{2.4}In_{2.4}O_{19}$	16.842	13.570	14.466	16.973	23.690	14.460
4	$PbFe_{2.4}Cu_{2.4}Sn_{2.4}Ga_{2.4}In_{2.4}O_{19}$	14.817	12.674	24.012	14.933	20.843	12.722

The initial components were weighed according to the stoichiometric ratio and processed in a planetary ball mill at 900 rpm for 5 hours and 10 hours using zirconiajarand balls. The mixtures of oxides obtained after grinding were pressed into tablets 8 mm in diameter and 2 mm high on a hydraulic laboratory press in a metal mold with a force of 5 t/cm^2. The weight of the tablets averaged about 1 gram. The obtained samples were placed on a platinum substrate and sintered in a laboratory muffle furnace with ferrochromium heaters. Heating was carried out according to the following scheme: (i) heating to 150 °C and holding at this temperature for 30 minutes, (ii) heating up to 500 °C and holding at this temperature for 30 minutes, (iii) heating up to 800 °C and holding at this temperature for 30 minutes, (iv) heating up to 900 °C and holding at this temperature for 60 minutes, (v) heating up to 1000 °C and holding at this temperature for 120 minutes, (vi) heating up to 1150 °C, holding for 15 minutes and cooling the samples in air. Such a stepwise regime provides gradual access to the temperature range at which PbO melts, other oxides dissolve in the resulting microdroplets, and double oxides form. It was assumed that one-hour exposure at 900 °C allows all or most of the molten PbO to react with the formation of stable binary oxides and this will serve as an obstacle to the evaporation of PbO at higher temperatures. Despite the measures taken, the evaporation of the components of the reaction mixture could become a key problem in the synthesis, therefore, the samples were weighed with an accuracy of 1 mg before and after heat treatment in order to control the results of the synthesis.

The synthesized samples, as a result of the chemical reaction, were studied by X-ray diffraction (XRD), scanning electron microscopy (SEM) equipped with energy dispersive spectroscopy (EDS). X-ray patterns were recorded on a Rigaku Ultima IV powder diffractometer using Cu-Kα radiation filtered by a Ni filter. The parameters of the elementary crystal lattice were also calculated from the data of powder X-ray diffraction patterns for samples 2. The calculation was made using the PDXL software package using a full profile analysis according to the Rietfeld method. The chemical composition and microstructure were studied on JEOL JSM-7001F and JSM-6460LV scanning electron microscopes equipped with Oxford Instruments energy dispersive analyzers.

3. Results and discussion

The main results of studying the compositions (chemical composition obtained by EDS, and phase analysis determined by XRD) of the obtained samples are presented in Table 2. It also presents the values that characterize the process of obtaining samples: the processing time for the mixture of starting materials in a planetary mill and the weight loss of the samples during the firing process. Comparison of the data presented in Tables 1, 2, as well as X-ray diffraction patterns and SEM images of the obtained material, allows us to come to the following conclusions. In all cases, the obtained samples contain large amount of oxide phases with the magnetoplumbite structure. A correlation is observed between the mass loss of the sample during its calcination and the phase purity of the obtained samples. For compositions "1" and "4", where the synthesis process was accompanied by maximum losses, PbO was clearly not enough to transform the entire substance into an oxide phase with the magnetoplumbite structure. This situation could be developed for three reasons (possibly different for samples "1" and "4"):

1. An oxide with magnetoplumbite structure could not be formed from composition "4".
2. Oxides with a given structure of magnetoplumbite did not have time to form during the heat treatment, which facilitated the process of evaporation of unbound PbO.
3. The obtained phases turned out to be insufficiently resistant to the temperatures used and partly dissociated with the evaporation of PbO. In this case, the synthesis process would probably be more successful with a reduction in heat treatment time.

The effect of milling time on the synthesis of the samples is not obvious. Judging by the results of powder diffractometry (Figs. 2 and 3 show the results for compositions "2" and "3", a similar picture is observed for other compositions), an increase in the milling time from 5 to 10 hours has practically no effect on the synthesis results. The same can be said by comparing the weight loss of the samples. There is no clear relationship between grinding time and weight loss.

TABLE 2. Chemical and phase compositions of the obtained samples

#	Mill time, h	Mass loss during synthesis, %	Composition of detectable phases according to EDS	Phase composition according to XRD (closest structures)
1	5	9.5	$PbFe_{12}O_{19}$+Fe_2O_3	$PbFe_{12}O_{19}$+Fe_2O_3
	10	11		
2	5	1	$PbFe_{2.4}Al_{2.6}Cr_{2.5}Ga_{2.3}In_{2.2}O_{19}$	$PbFe_{12}$ O_{19}
	10	3	$PbFe_{2.4}Al_{2.6}Cr_{2.5}Ga_{2.2}In_{2.3}O_{19}$	
3	5	4.5	$PbFe_{2.3}Co_{2.6}Ti_{2.5}Ga_{2.3}In_{2.3}O_{19}$	$PbFe_{12}O_{19}$ + ?
	10	3	$PbFe_{2.4}Co_{2.5}Ti_{2.5}Ga_{2.2}In_{2.4}O_{19}$	
4	5	7.5	$PbFe_{2.4-3.2}Cu_{2.0-3.5}Sn_{1.2-1.9}Ga_{2.1-3.3}In_{1.5-3.0}O_{19}$+ +$SnO_2$	$PbFe_{12}O_{19}$+$GaInO_3$+ +SnO_2+$Cu_{0.75}Fe_{2.25}O_4$
	10	6.5		

Judging by the X-ray diffraction data of $PbFe_{2.4}Al_{2.4}Cr_{2.4}Ga_{2.4}In_{2.4}O_{19}$ (Fig. 2), single-phase samples of high-entropy phases with the magnetoplumbite structure were obtained. For these samples, the unit cell parameters were calculated, it is presented in Table 3. These parameters can be compared with the literature data on the parameters for Pb, Ba, and Sr hexaferrites. It can be seen that the obtained data lie within the range of these values.

For the system, its composition is reflected by $PbFe_{2.4}Co_{2.4}Ti_{2.4}Ga_{2.4}In_{2.4}O_{19}$, samples with a predominance high-entropy magnetoplumbite phase were obtained, but a small amount of impurities is also present. Comparison of the data in Fig. 3 with the available XRD patterns of compounds that can be formed from the constituent elements of $PbFe_{2.4}Co_{2.4}Ti_{2.4}Ga_{2.4}In_{2.4}O_{19}$ suggests that the impurity is Pb_2O_3. However, this contradicts to the detected mass

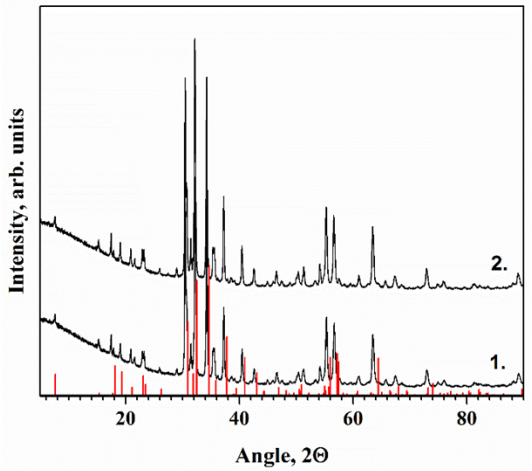

FIG. 2. Powder diffraction patterns for samples "2" at 300 K after 5 h (1) and 10 h (2) milling time. Red columns are reference data for $PbFe_{12}O_{19}$ [38]

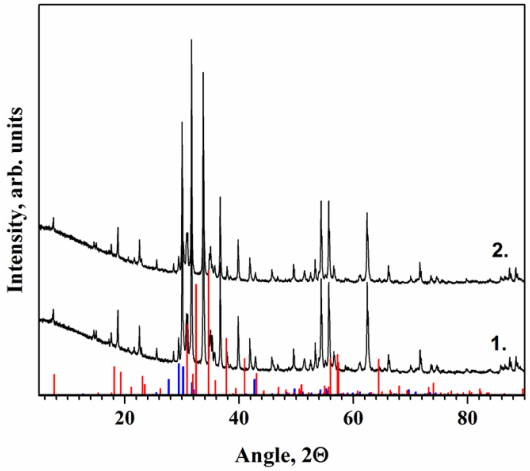

FIG. 3. Powder diffraction patterns for samples "3" at 300 K after 5 h (1) and 10 h (2) milling time. Red bars are reference data for $PbFe_{12}O_{19}$ [38], blue bars are for Pb_2O_3 [40]

TABLE 3. Unit cell parameters of samples of compositions "2"

Sample	a, Å	c, Å	V, Å^3
$PbFe_{2.4}Al_{2.4}Cr_{2.4}Ga_{2.4}In_{2.4}O_{19}$, 5 hours	5.858	23.227	690.4
$PbFe_{2.4}Al_{2.4}Cr_{2.4}Ga_{2.4}In_{2.4}O_{19}$, 10 hours	5.863	23.272	692.8
$PbFe_{12}O_{19}$ [38]	5.780	23.090	668.052
$BaFe_{12}O_{19}$ [39]	5.893	23.194	697.50
$SrFe_{12}O_{19}$ [39]	5.780	22.980	664.80

loss (Table 2), which indicates the samples lose PbO during heat treatment, as well as the data of electron microscopy did not allow detection of segregated Pb_2O_3 particles.

The available data (both those obtained in the course of the study and literature data on the properties of the substances involved in the ongoing processes) suggest that the synthesis mechanism includes the melting of PbO microparticles in the initial mixture and the dissolution of other oxides in the liquid phase with the formation of oxide particles (including multicomponent) with the structure of magnetoplumbite.

Figure 4 shows SEM images of the obtained samples at magnification $\times$25000 (for samples "2") and $\times$10000 (for samples "3"). The samples have a porous typical structure of ceramics. In the presented images, particles with natural faceting are clearly visible. The particles have a hexagonal faceting typical of materials with the magnetoplumbite structure. The results of the electron microscopy study of samples "2" did not allow us to detect particles that differ significantly in composition and morphology from the main matrix phase. This testifies in favor of the conclusion that single-phase samples were obtained in this case. In samples "3", there is a small number of small particles with a nearly cubic shape, but their size does not allow us to determine their composition using EDS.

The data presented in Fig. 4, among other things, demonstrate that relatively low temperatures made it possible to obtain crystallites whose dimensions for composition "2" are of the order of 100 nm or less (considering the thickness of hexagonal plates). In samples "1" and "4", the size of crystallites of oxide phases with the magnetoplumbite structure are much larger. This can be judged by the images presented in Fig. 5.

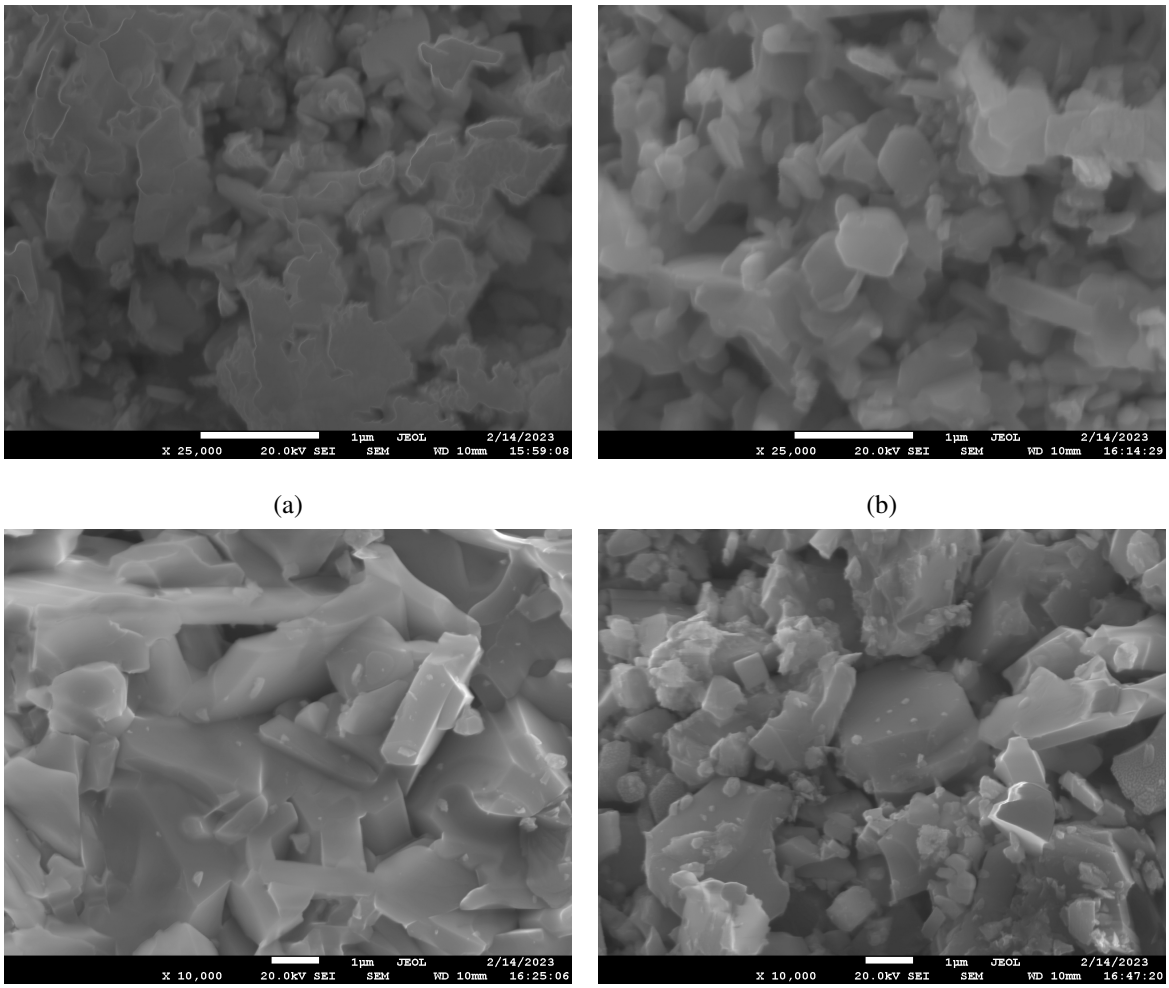

FIG. 4. SEM images of sample microstructures: (a) $PbFe_{2.4}Al_{2.4}Cr_{2.4}Ga_{2.4}In_{2.4}O_{19}$ (5 hours), (b) $PbFe_{2.4}Al_{2.4}Cr_{2.4}Ga_{2.4}In_{2.4}O_{19}$ (10 hours), (c) $PbFe_{2.4}Co_{2.4}Ti_{2.4}Ga_{2.4}In_{2.4}O_{19}$ (5 hours), (d) $PbFe_{2.4}Co_{2.4}Ti_{2.4}Ga_{2.4}In_{2.4}O_{19}$ (10 hours)

4. Conclusions

1. For the first time, single-phase samples of high-entropy phases with the magnetoplumbite structure were obtained, the composition of which is reflected by the formula $PbFe_{2.4}Al_{2.4}Cr_{2.4}Ga_{2.4}In_{2.4}O_{19}$. The particle size of the high-entropy phase is about 100 nm, which makes them promising for a number of applications. For the composition, which is reflected by the formula $PbFe_{2.4}Co_{2.4}Ti_{2.4}Ga_{2.4}In_{2.4}O_{19}$, samples were obtained in which the high-entropy phase with the magnetoplumbite structure predominates.
2. The conditions for the synthesis of the resulting phases have been established. The effect of preliminary ball milling of the initial components has been studied. A synthesis mechanism is proposed.
3. The results of the study pave the way to synthesis and study of the properties of a new large subgroup of high-entropy oxides with the magnetoplumbite structure, which expands the possibilities of controlling the properties of ceramic functional materials.

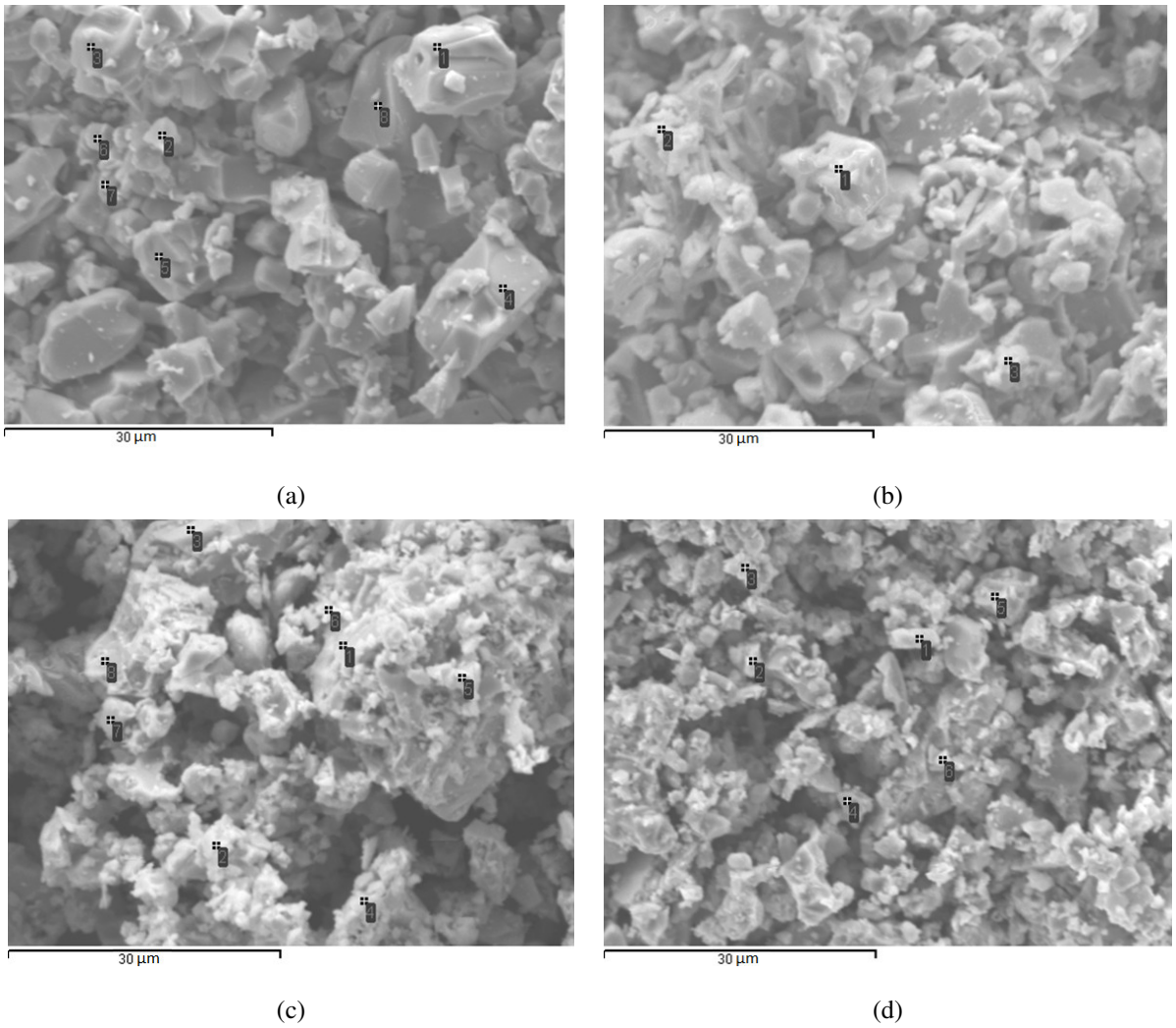

(a) (b)

(c) (d)

FIG. 5. SEM images showing the microstructures of (a) $PbFe_{12}O_{19}$ (5 hours), (b) $PbFe_{12}O_{19}$ (10 hours), (c) $PbFe_{2.4}Cu_{2.4}Sn_{2.4}Ga_{2.4}In_{2.4}O_{19}$ (5 hours), (d) $PbFe_{2.4}Cu_{2.4}Sn_{2.4}Ga_{2.4}In_{2.4}O_{19}$ (10 hours)

References

[1] Wang C., Ma X., Xu C., Chen H., Chen Y., Chen F., Kang B., Lu W., Zhang J., Cao S. Magnetic field-induced polarization reversal in Y-type hexaferrites single crystals. *Ceram. Int.*, 2021, **47**, P. 19356–19361.

[2] Huang K., Yu J., Zhang L., Xu J., Yang Z., Liu C., Wang W., Kan X. Structural and magnetic properties of Gd–Zn substituted M-type Ba–Sr hexaferrites by sol-gel auto-combustion method. *J. Alloys Compd.*, 2019, **803**, P. 971–980.

[3] Zhang W., Li J., Yi S., Zu P., Wu J., Lin J., Li M., Su W. Influence of La–Nb co-substituted Sr ferrite on microstructure, spectrum and magnetic properties of hexaferrites. *J. Alloys Compd.*, 2021, **871**, 159563.

[4] Almessiere M.A., Slimani Y., Algarou N.A., Gondal M.A., Wudil Y.S., Younas M., Auwal I.A., Baykal A., Manikandan A., Zubar T.I., Kostishin V.G., Trukhanov A.V., Ercan I. Electronic, magnetic, and microwave properties of hard/soft nanocomposites based on hexaferrite $SrNi_{0.02}Zr_{0.02}Fe_{11.96}O_{19}$ with variable spinel phase MFe_2O_4 (M=Mn, Co, Cu and Zn). *Ceram. Int.*, 2021, **47**, P. 35209–35223.

[5] Darwish M.A., Turchenko V.A., Morchenko A.T., Kostishyn V.G., Timofeev A.V., Sayyed M.I., Sun Z., Podgornaya S.V., Trukhanova E.L., Kaniukov E.Y., Trukhanov S.V., Trukhanov A.V. Heterovalent substituted $BaFe_{12-x}Sn_xO_{19}$ ($0.1 \leq x \leq 1.2$) M-type hexaferrite: Chemical composition, phase separation, magnetic properties and electrodynamics features. *J. Alloys Compd.*, 2022, **896**, 163117.

[6] Shams M.H., Salehi S.M.A., Ghasemi A. Electromagnetic wave absorption characteristics of Mg–Ti substituted Ba-hexaferrite. *Mater. Lett.*, 2008, **62** (10–11), P. 1731–1733.

[7] Millimetre wave and terahertz sensors and technology XIII. Salmon N.A., Gumbmann F. (ed.) *Proc. SPIE – Int. Soc. Opt. Eng.*, 2020, **11541**, 121 p.

[8] Bhaduri A., Singh S., Thapa K.B., Yadav B.C. Visible light-induced, highly responsive, below lower explosive limit (LEL) LPG sensor based on hydrothermally synthesized barium hexaferrite nanorods. *Sensors Actuators B Chem.*, 2021, **348**, 130714.

[9] Rajaji U., Chinnapaiyan S., Chen T.-W., Chen S.-M., Mani G., Mani V., Ali M.A., Al-Hemaid F.M.A., El-Shikh M.S. Rational construction of novel strontium hexaferrite decorated graphitic carbon nitrides for highly sensitive detection of neurotoxic organophosphate pesticide in fruits. *Electrochim. Acta*, 2021, **371**, 137756.

[10] Rai G.M., Iqbal M.A., Kubra K.T. Effect of Ho^{3+} substitutions on the structural and magnetic properties of $BaFe_{12}O_{19}$ hexaferrites. *J. Alloys Compd.*, 2010, **495**, P. 229–233.

[11] Jacobo S.E., Hermea C., Bercoff P.G. Influence of the iron content on the formation process of substituted Co–Nd strontium hexaferrite prepared by the citrate precursor method. *J. Alloys Compd.*, 2010, **495**, P. 513–515.
[12] Thakur A., Singh R.R., Barman P.B. Structural and magnetic properties of La^{3+} substituted strontium hexaferrite nanoparticles prepared by citrate precursor method. *J. Magn. Magn. Mater.*, 2012, **326**, P. 35–40.
[13] Kostishyn V.G., Panina L.V., Timofeev A.V., Kozhitov L.V., Kovalev A.N., Zyuzin A.K. Dual ferroic properties of hexagonal ferrite ceramics $BaFe_{12}O_{19}$ and $SrFe_{12}O_{19}$. *J. Magn. Magn. Mater.*, 2016, **400**, P. 327–332.
[14] Pullar R.C. Hexagonal ferrites: A review of the synthesis, properties and applications of hexaferrite ceramics. *Prog. Mater. Sci.*, 2012, **57** (7), P. 1191–1334.
[15] Gorbachev E.A., Trusov L.A., Wu M., Vasiliev A.V., Svetogorov R.D., Alyabyeva L.N., Lebedev V.A., Sleptsova A.E., Karpov M.A., Mozharov Y.M., Gorshunov B.P., Kazin P.E. Submicron particles of Ga-substituted strontium hexaferrite obtained by a citrate auto-combustion method. *J. Mater. Chem. C*, 2021, **9**, P. 13832–13840.
[16] Choi J.-Y., Baek Y.-K., Lee J.-G., Kim Y.-K. Effect of sodium addition on structural and magnetic properties of solid state processed $SrFe_{12-x}Al_xO_{19}$ ($x \leq 4$). *Appl. Phys. A: Mater. Sci. and Proces.*, 2022, **128** (12).
[17] Wu C., Liu Q., Yin Q., Chen J., Zhang H., Liu Y. Room-temperature multiferroic properties of Al-doped hexaferrites sintered at high oxygen atmospheric concentrations. *Ceram. Int.*, 2021, **47** (15), P. 21398–21403.
[18] Sözeri H., Genç F., Almessiere M.A., Ünver İ.S., Korkmaz A.D., Baykal A. CR^{3+}-substituted Ba nanohexaferrites as high-quality microwave absorber in X band. *J. Alloys Compd.*, 2019, **779**, P. 420–426.
[19] Turchenko V., Kostishin V.G., Trukhanov S., Damay F., Balasoiu M., Bozzo B., Fina I., Burkhovetsky V.V., Polosan S., Zdorovets M.V., Kozlovskiy A.L., Astapovich K.A., Trukhanov A. Structural features, magnetic and ferroelectric properties of $SrFe_{10.8}In_{1.2}O_{19}$ compound. *Mater. Res. Bull.*, 2021, **138**, 111236.
[20] Huang, K., Yu, J., Zhang, L., Xu, J., Li, P., Yang, Z., Kan, X. Synthesis and characterizations of magnesium and titanium doped M-type barium calcium hexaferrites by a solid state reaction method. *J. Alloys Comp.*, 2020, **825**, 154072.
[21] Vinnik D. A., Gudkova S.A., Zhivulin V.E., Trofimov E.A. Ferrite-based solid solutions: Structure types, preparation, properties, and potential applications. *Inorg. Mater.*, 2021, **57** (11), P. 1109–1118.
[22] Zhilina E.M., Russkikh A.S., Krasikov S.A., Osinkina T.V., Rempel A.A. Synthesis of High-Entropy Alloy AlTiZrVNb by Aluminothermic Reaction. *Inorg. Chem.*, 2022, **67** (6), P. 825–828.
[23] Teplonogova M.A, Yapryntsev A.D., Baranchikov A.E., Ivanov V.K. High-entropy layered rare earth hydroxides. *Inorg. Chem.*, 2022, **61** (49), P. 19817–9827.
[24] Wang B., Yao J., Wang J., Chang A. Spinel-type high-entropy $(Co_{0.2}Mn_{0.2}Fe_{0.2}Zn_{0.2}Ti_{0.2})_3O_4$ oxides constructed from disordered cations and oxygen vacancies. *J. Alloys Compd.*, 2022, **897**, 163188.
[25] Vinnik D.A., Zhivulin V.E., Trofimov E.A., Gudkova S.A., Punda A.Y., Valiulina A.N., Gavrilyak M., Zaitseva O.V., Taskaev S.V., Khandaker M.U., Alqahtani A., Bradley D.A., Sayyed M.I., Turchenko V.A., Trukhanov A.V., Trukhanov S.V. A-site cation size effect on structure and magnetic properties of $Sm(Eu,Gd)Cr_{0.2}Mn_{0.2}Fe_{0.2}Co_{0.2}Ni_{0.2}O_3$ high-entropy solid solutions. *Nanomaterials*, 2022, **12** (1), 36.
[26] Dabrowa J., Cieślak J., Zajusz M., Moździerz M., Berent K., Mikula A., Stepień A., Świerczek K. Structure and transport properties of the novel $(Dy,Er,Gd,Ho,Y)_3Fe_5O_{12}$ and $(Dy,Er,Gd,Ho,Y)_3Fe_5O_{12}$ high entropy garnets. *J. Eur. Ceram. Soc.*, 2021, **41**, P. 3844–3849.
[27] Vinnik D.A., Trofimov E.A., Zhivulin V.E., Zaitseva O.V., Gudkova, S.A., Starikov A.Y., Zherebtsov D.A., Kirsanova A.A., Hässner M., Niewa R. High-entropy oxide phases with magnetoplumbite structure. *Ceram. Int.*, 2019, **45** (10), P. 12942–12948.
[28] Vinnik D.A., Trofimov E.A., Zhivulin V.E., Zaitseva O.V., Zherebtsov D.A., Starikov A.Y., Sherstyuk D.P., Gudkova S.A., Taskaev S.V. The new extremely substituted high entropy $(Ba,Sr,Ca,La)Fe_{6-x}(Al,Ti,Cr,In,Cu,W)_xO_{19}$ microcrystals with magnetoplumbite structure. *Ceram. Int.*, 2020, **46** (7), P. 9656–9660.
[29] Vinnik D.A., Zhivulin V.E., Trofimov E.A., Starikov A.Y., Zherebtsov D.A., Zaitseva O.V., Gudkova S.A., Taskaev S.V., Klygach D.S., Vakhitov M.G., Sander E.E., Sherstyuk D.P. Trukhanov A.V. Extremely polysubstituted magnetic material based on magnetoplumbite with a hexagonal structure: Synthesis, structure, properties, prospects. *Nanomater.*, 2019, **9** (4).
[30] Trukhanov A.V., Vinnik D.A., Trofimov E.A., Zhivulin V.E., Zaitseva O.V., Taskaev S.V., Zhou D., Astapovich K.A., Trukhanov S.V., Yang Y. Correlation of the Fe content and entropy state in multiple substituted hexagonal ferrites with magnetoplumbite structure. *Ceram. Int.*, 2021, **47**, P. 17684–17692.
[31] Zhivulin V.E., Trofimov E.A., Zaitseva O.V., Sherstyuk D.P., Cherkasova N.A, Taskaev S.V., Vinnik D.A., AlekhinaYu.A., Perov N.S., Tishkevich D.I., Zubar T.I., Trukhanov A.V., Trukhanov S.V. Effect of configurational entropy on phase formation, structure, and magnetic properties of deeply substituted strontium hexaferrites. *Ceram. Int.*, 2023, **49** (1), P. 1069–1084.
[32] Obradors X., Solans X., Collomb A., Samaras D., Rodriguez J., Pernet M., Font-Altaba M. Crystal structure of strontium hexaferrite $SrFe_{12}O_{19}$. *J. Sol. St. Chem.*, 1988, **72** (2), P. 218–224.
[33] Vinnik D.A., Trofimov E.A., Zherebtsov D.A. Experimental Study and Thermodynamic Modeling of Phase Equilibria in PbO–Fe_2O_3 System. In *Materials Science Forum Trans Tech Publications, Ltd.*, 2016, **870**, P. 282–285.
[34] Nevřiva M., Fischer K. Contribution to the binary phase diagram of the system PbO–Fe_2O_3. *Mater. Res. Bull.*, 1986, **21**, P. 1285–1290.
[35] Jonker H.D. Investigation of the phase diagram of the system PbO–B_2O_3–Fe_2O_3–Y_2O_3 for the growth of single crystals of $Y_3Fe_5O_{12}$. *J. Cryst. Growth.*, 1975, **28**, P. 231–239.
[36] Mountvala A.J., Ravitz S.F. Phase Relations and Structures in the System PbO–Fe_2O_3. *J. Am. Ceram. Soc.*, 1962, **45**, P. 285–288.
[37] Diop I., David N., Fiorani J.M., Podor R., Vilasi M. Experimental investigations and thermodynamic description of the PbO–Fe_2O_3 system. *Thermochimica Acta*, 2010, **510**, P. 202–212.
[38] Aleshko-Ozhevskii O.P., Faek M.K., Yamzin I.I. A neutron diffraction study of the structure of magnetoplumbite. *Soviet Physics – Crystallography*, 1969, **14**, P. 367–369.
[39] Obradors X., Collomb A., Pernet M., Samaras D., Joubert J.C. X-ray analysis of the structural and dynamic properties of $BaFe_{12}O_{19}$ hexagonal ferrite at room temperature. *J. Solid State Chem.*, 1985, **56** (2), P. 171–181.
[40] Bouvaist J., Weigel D. Sesquioxyde de plomb, Pb_2O_3. I. Determination de la structure. *Acta Crystallogr. A*, 1970, **26**, P. 501–510.

Submitted 19 March 2023; revised 9 April 2023; accepted 10 April 2023

Information about the authors:

Olga V. Zaitseva – South Ural State University, Lenin Av., 76, Chelyabinsk, 454080, Russia;
ORCID 0000-0001-5888-3297; zaitcevaov@susu.ru

Evgeny A. Trofimov – South Ural State University, Lenin Av., 76, Chelyabinsk, 454080, Russia;
ORCID 0000-0001-8073-3244; trofimovea@susu.ru

Vladimir E. Zhivulin – South Ural State University, Lenin Av., 76, Chelyabinsk, 454080, Russia;
ORCID 0000-0002-4389-8936; zhivulinve@mail.ru

Ahmad Ostovari Mogaddam – South Ural State University, Lenin Av., 76, Chelyabinsk, 454080, Russia;
ORCID 0000-0002-5316-3773; ostovarim@susu.ru

Olga V. Samoilova – South Ural State University, Lenin Av., 76, Chelyabinsk, 454080, Russia;
ORCID 0000-0002-9514-3201; samoylova_o@mail.ru

Ksenia S. Litvinyuk – South Ural State University, Lenin Av., 76, Chelyabinsk, 454080, Russia;
ORCID 0009-0002-4773-1372; xenialitvinyuk@gmail.com

Alena R. Zykova – South Ural State University, Lenin Av., 76, Chelyabinsk, 454080, Russia;
ORCID 0000-0001-6333-5551; zykovaar@susu.ru

Dmitry V. Mikhailov – South Ural State University, Lenin Av., 76, Chelyabinsk, 454080, Russia;
ORCID 0000-0003-2484-8076; a_b_c81@mail.ru

Svetlana A. Gudkova – South Ural State University, Lenin Av., 76, Chelyabinsk, 454080, Russia;
ORCID 0000-0002-3028-947X; svetlanagudkova@yandex.ru

Denis A. Vinnik – South Ural State University, Lenin Av., 76, Chelyabinsk, 454080, Russia;
ORCID 0000-0002-5190-9834; vinnikda@susu.ru

Conflict of interest: the authors declare no conflict of interest.